Gelation on the microscopic scale

Felix K. Oppong,[1,*] P. Coussot,[2,†] and John R. de Bruyn[1,‡]
[1]*Department of Physics and Astronomy, University of Western Ontario, London, Ontario, Canada N6A 3K7*
[2]*Université Paris-est, Institut Navier, 77420 Champs sur Marne, France*
(Received 5 March 2008; published 26 August 2008)

Particle-tracking methods are used to study gelation in a colloidal suspension of Laponite clay particles. We track the motion of small fluorescent polystyrene spheres added to the suspension, and obtain the micron-scale viscous and elastic moduli of the material from their mean-squared displacement. The fluorescent spheres move subdiffusively due to the microstructure of the suspension, with the diffusive exponent decreasing from close to one at early times to near zero as the material gels. The particle-tracking data show that the system becomes more heterogeneous on the microscopic scale as gelation proceeds. We also determine the bulk-scale moduli using small-amplitude oscillatory shear rheometry. Both the macroscopic and microscopic moduli increase with time, and on both scales we observe a transition from a primarily viscous fluid to an elastic gel. We find that the gel point, determined as the time at which the viscous and elastic moduli are equal, is length-scale dependent—gelation occurs earlier on the bulk scale than on the microscopic scale.

DOI: 10.1103/PhysRevE.78.021405 PACS number(s): 82.70.Dd, 83.60.Pq

I. INTRODUCTION

Aqueous suspensions of colloidal clay particles have many industrial applications, including drilling fluids, paints, ceramics, cosmetics, and pharmaceutical products. Clay suspensions have also attracted much fundamental interest due to their rich phase behavior and interesting mechanical properties [1]. Clay suspensions also show rheological aging [2], that is, their mechanical properties change significantly over time. The bulk-scale behavior of these materials derives from microscopic-scale interactions among the suspended particles, and a comprehensive understanding of their behavior thus requires an understanding of the relationship between structure and properties on these two very different length scales.

In this work we examine the gelation over time of a suspension of Laponite in water by tracking the thermally driven motion of micron-scale tracer particles [3–6]. Laponite is a synthetic clay consisting of disklike particles 30 nm in diameter and 1 nm in thickness. It is commonly used as a model system for studying yield stress and aging phenomena in complex fluids. The suspended Laponite particles are charged and interact via both electrostatic and van der Waals forces. The strength of the electrostatic interactions can be tuned by changing the concentration of ions in the suspension, making both gel and glass phases possible [7,8]. At low ionic strength, electrostatic repulsion dominates and Laponite forms a glass, while a higher concentration of ions screens the electrostatic interactions allowing formation of an attractive gel phase. These soft solid phases can form at particle volume fractions of order a few tenths of a percent, compared to about 50% for uncharged colloidal particles and hard sphere suspensions. The work reported here is done at a relatively high ionic strength, in the regime in which Laponite forms a gel.

The gelation transition from the predominantly viscous fluid (sol) phase to the primarily elastic gel phase is a percolation transition at which the interparticle interactions result in the formation of an extensive fractal aggregate that spans the whole system [1,9–12]. Gelation has also been discussed in terms of a jamming transition [13]. The nature of the gel-formation process and of gel phases formed under different conditions is complex, and has been discussed in detail in a recent review paper [12]. The viscoelastic properties of a variety of materials have been studied near the gel transition by applying a small-amplitude oscillatory shear to the material. The resulting stress is measured as a function of frequency. Chambon and Winter first reported that the viscous and elastic moduli of polydimethylsiloxane, a chemical gel, showed the same power-law scaling over a wide range of frequencies at a particular age, which they identified as the gel point [14,15]. Similar behavior has been observed at the gel point of many chemical and physical gels [15–20]. The zero-frequency viscosity in the sol phase displays a power-law divergence as a function of frequency as the gel transition is approached, while the equilibrium shear modulus shows a continuous power-law increase from zero in the gel phase. Dynamic light scattering has also been used to study aging and the gelation process on a microscopic scale [19,21–26]. The temporal autocorrelation function of the scattered light intensity shows a power-law decay with time at the gel point. In both cases the power-law behavior indicates that relaxation occurs on all time scales at the gel transition.

Several experimental studies have been performed on Laponite suspensions, mainly using scattering techniques [8,22,25–39] and bulk rheological measurements [29,40–42]. Kroon *et al.* performed dynamic light scattering studies on the sol-gel transition in Laponite [23]. They found that the transition is marked by a change in the intensity of the scattered light with the autocorrelation function of the scattered intensity showing relaxation times stretching over more than five orders of magnitude. Ruzicka *et al.* [8,25] observed different routes to gelation as a function of clay concentration and found that the arrested state was inhomogeneous at low

*foppong@uwo.ca
†coussot@lcpc.fr
‡debruyn@uwo.ca

concentration and homogeneous at higher concentration. Rheological measurements have shown that the sol-gel transition shifts to lower volume fractions with increasing ionic strength [29]. The viscous and elastic moduli of gelling Laponite suspensions showed a power-law frequency dependence at a well-defined gel time, suggesting that the gelation was due to the formation and growth of self-similar clusters [41], consistent with the percolation model. Pignon *et al.* proposed that Laponite gels form a fractal network made up of aggregates which are themselves on the order of a micron in size [22,31]. The age-dependence of the local rheology of a Laponite suspension was studied using a small magnetic probe [43]. Recently a combination of active and passive microrheological measurements performed using optical tweezers were used to validate the fluctuation-dissipation theorem in an aging Laponite suspension [44].

The technique used in the present work is particle-tracking microrheology, which makes use of the thermally driven diffusive motion of tracer particles suspended in the material of interest to probe its local viscoelastic properties [3–6]. With the aid of the fluctuation-dissipation theorem, the local linear viscoelastic moduli are calculated from the mean-squared displacement of the tracer particles [4]. The particle-tracking technique probes the linear viscoelastic response of the material to thermal fluctuations on the length scale of the tracer particles. When the particles are large compared to the characteristic length scale of any structure in the fluid, the viscoelastic moduli calculated in this way will be the same as those measured on the bulk scale. On the other hand, if the particles are small compared to any structure, the microrheological moduli will characterize the local environment in which the particles move. Finally, if the two length scales are comparable, then particle tracking provides information about the structure and viscoelastic properties of the material on that length scale. Recently, particle-tracking microrheology has been used to study the properties of a variety of gel systems, including attractive colloidal particles [45], Carbopol, a polymer microgel [46,47], a hectorite clay suspension [48], and gellan gum [49]. We use particle-tracking methods to monitor the gelation of a Laponite suspension over time. From the mean-squared displacement of the tracer particles we determine the viscous and elastic moduli of the suspension on the microscopic scale and obtain information about the evolution of the small-scale structure of the material as it gels. By comparing our microrheological results to those from bulk-scale shear rheometry, we demonstrate that the time scale for gelation is longer on smaller length scales. The details of our experiments are given Sec. II. The results are presented in Sec. III and discussed in Sec. IV. Section V is a brief conclusion.

II. EXPERIMENT

A. Sample preparation

The material used in this study is Laponite RD (Southern Clay Products, Gonzales, TX), a synthetic hectorite clay made up of disk-shaped particles approximately 30 nm in diameter and 1 nm thick. Its chemical formula is $Si_8[Mg_{5.5}Li_{04}H_{4.0}O_{24.0}]^{-0.7}Na^{+0.7}_{0.7}$. 10^{-3} mol/l NaCl was added to distilled, deionized water. Laponite powder was then dispersed in this solution at a concentration of 1% by weight (corresponding to 0.4% by volume, where we have taken the density of the Laponite particles to be 2.53 g/cm^3 [50]) and mixed thoroughly overnight. The salt serves to control the ionic strength of the suspension and screen the long-range electrostatic interactions between clay particles. The *p*H of the suspension was then adjusted to 10 by addition of NaOH to inhibit the dissolution of the clay particles [28,51]. The purpose of the present experiments was to compare gelation of the Laponite suspension on the microscopic and macroscopic length scales. We started the measurements from an initial fluidized state in which any preexisting microstructure had been destroyed. Laponite undergoes irreversible changes in material properties over long times as a result of slow chemical reactions with atmospheric gases, particularly CO_2. To minimize the irreversible changes which occurred over the duration of our experiments, we covered the suspension after preparation and allowed it to stand for 1 month before measurements were made. The suspension was then subjected to strong stirring to break up the gel which formed over this period. Fluorescent polystyrene microspheres (Duke Scientific, Freemont, CA) of radius 0.50 μm, density 1.05 g/cm^3, and refractive index 1.59 were then added to the suspension and stirring was continued for 8 h to ensure that the spheres were completely mixed in to the sample. The suspension was then covered and left undisturbed overnight. Material from this sample was used for both the particle-tracking and the bulk rheological measurements. Immediately prior to the start of the particle-tracking measurements, the sample was sonicated for approximately 30 min to break down any preexisting microstructure and to prepare the suspension in a reproducible fluid state which was the initial condition for our measurements. The aggregation time t_w is defined as the time from the end of the sonication to the start of the particle-tracking measurement.

Sample cells were made by gluing three small glass bars cut from a microscope slide onto a second slide with optical cement to form a U-shaped wall of dimensions $10\times10\times0.75$ mm^3. A cover slip was then glued to the top of this wall to form a chamber with a volume of approximately 0.075 cm^3. The Laponite samples were loaded into the cells with a glass dropper, and the cells then sealed with an inert silicone grease.

B. Video microscopy and multiple particle tracking

The fluorescent microspheres suspended in the Laponite samples were imaged using an inverted fluorescence microscope (Nikon Eclipse TE 2000U) with a 40× objective. To minimize the influence of the cell walls, the microscope was focused at the vertical midpoint of the cell and far from the lateral walls. At any time, 30–50 particles were present in the microscope's field of view. A charge-coupled-device camera was used to capture images of the tracer particles for 50 s at a rate of 10 video frames per second. Since the duration of the measurement is always much less than t_w, changes in materials properties over the course of the measurement are insignificant. The spatial resolution and scale of the images

was determined using an etched calibration slide. The resolution was higher in one direction (which we define as the x direction) than the other because of the way in which the camera records images; the resolution in the x direction was 0.33 μm/pixel. Measurements were made at a temperature of 22 ± 0.1 °C.

The video images were stored directly on a personal computer and analyzed following the experiment to obtain the positions and trajectories of the tracer particles using image processing software described in detail in Refs. [52,53]. From the trajectories, we calculated the one-dimensional mean-squared displacement of the tracer particles in the x direction, $\langle x^2(\tau)\rangle = \langle |x(t+\tau) - x(t)|^2 \rangle$. Here t is an arbitrary starting time and τ a lag time between data points. The angle brackets indicate an ensemble average over all particles as well as over all starting times.

The viscous and elastic moduli of the material on the length scale sampled by the tracer particles can be calculated from $\langle x^2(\tau)\rangle$ using a generalized Stokes-Einstein relation [3,4]. This relation is derived under the assumption that the inertia of the tracer particles can be neglected, and that the tracer particles are much larger than any microstructure in the material. In this formulation, the magnitude of the frequency-dependent complex modulus is given by [4]

$$|G(\omega)| = \frac{k_B T}{\pi a \langle r^2(1/\omega)\rangle \Gamma(1+\alpha(\omega))}, \tag{1}$$

where k_B is the Boltzmann constant, T the temperature, Γ the gamma function, and a the radius of the tracer particles. $\alpha(\omega)$ is the frequency-dependent logarithmic slope of the mean squared displacement and is evaluated at reciprocal time $\omega = 1/\tau$ as

$$\alpha(\omega) = \left. \frac{d \ln\langle r^2(\tau)\rangle}{d \ln \tau} \right|_{\tau = 1/\omega}. \tag{2}$$

The microrheological viscous and elastic moduli, G_m'' and G_m', respectively, are given by [4]

$$G_m''(\omega) = |G(\omega)| \sin\left(\frac{\pi\alpha(\omega)}{2}\right) \tag{3}$$

and

$$G_m'(\omega) = |G(\omega)| \cos\left(\frac{\pi\alpha(\omega)}{2}\right). \tag{4}$$

The subscript m on the symbols for the moduli distinguishes them from the bulk-scale moduli introduced below.

Since the gel we study forms via a percolation transition, the material is expected to have structure on all scales ranging from the size of the basic building blocks of the percolation cluster to the size of the sample. Our 0.5 μm tracer particles are thus not large compared to the structural scale, so our particle-tracking experiments probe the properties of the suspension only on length scales up to the particle size. The viscous and elastic moduli determined from our particle tracking data are therefore not expected to be quantitatively the same as the bulk moduli obtained from the rheological measurements described below. Rather, they should be interpreted as "effective" moduli which characterize the viscoelastic properties of the material on the micron scale.

C. Bulk rheology

An Ares RHS strain-controlled rheometer (TA Instruments, New Castle, DE) was used for the bulk rheological measurements. We used a Couette cell, which consists of a cylindrical cup of diameter 34 mm in which a bob of diameter 32 mm and length 34 mm is inserted. The cup is rotated to apply the required deformation and the resulting stress is determined from the measured torque on the bob. This geometry was used because at the early stages of the experiment the samples have very low viscosity and are difficult to load into the alternative cone-and-plate or parallel plate geometries. The Laponite sample (including the added microspheres) was taken from the same batch of material used for the microscopic measurements. An environmental housing was placed over the open top of the Couette cell to maintain a humid atmosphere above the sample and to reduce evaporation or drying of the sample over the course of the experiments. The temperature of the rheometer tool was controlled with a temperature-controlled circulating fluid bath at 22 ± 0.1 °C.

To study the variation of the linear viscous and elastic moduli of the bulk material as it gels, we first presheared the sample at a shear rate $\dot{\gamma}$ of 100 s^{-1} for 60 s prior to the measurement. The preshear ensures that the material is in a fluidized state before the measurements. Measurements on samples presheared in this way, and on samples sonicated as in the particle-tracking experiments, showed that the two methods of preparing the material produced suspensions with very similar rheological properties and time evolution. For the bulk experiments, t_w was measured from the end of the preshear. We then applied a oscillatory strain with an amplitude of 0.05 and a frequency of 1 rad/s, and determined the bulk viscous and elastic moduli $G_b''(t_w)$ and $G_b'(t_w)$ from the amplitude and phase of the measured shear stress [1,54] as the material gelled. For this strain amplitude the suspension is in the linear viscoelastic regime, meaning that the strain is small enough that the structure of the material is not disrupted by the measurements and the moduli are independent of amplitude. We also measured G_b'' and G_b' as a function of the strain amplitude to monitor the transition from the linear to the nonlinear regime over the course of the gelation process. These two sets of measurements could both be carried out in a few minutes, ensuring that the sample did not age significantly over the course of the measurements. On the other hand, measurements of the flow curve (stress as a function of shear rate) took considerably longer and could not be used to determine the yield stress because the properties of the suspension changed over the time required to do the measurements. Instead we obtained a self-consistent estimate of the yield stress from the data for G_b' as described below.

III. RESULTS

Figure 1 shows the mean-squared displacement $\langle x^2(\tau)\rangle$ as a function of lag time τ for several different values of the

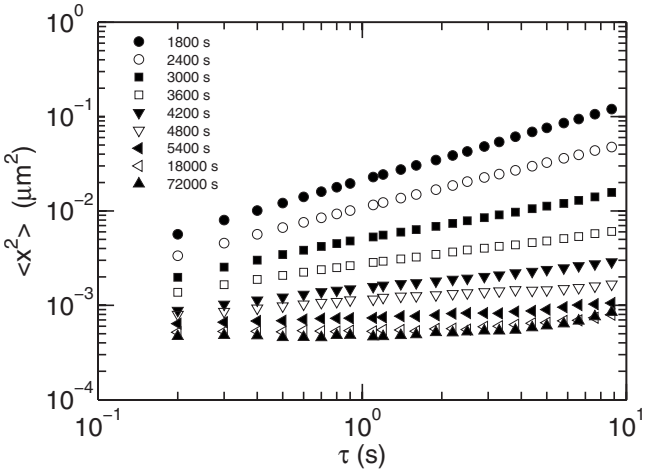

FIG. 1. The one-dimensional ensemble-averaged mean-squared displacement of the tracer particles as a function of lag time τ. The different symbols indicate the aggregation time t_w since preparation of the Laponite suspension.

aggregation time t_w. Over most of the range of the data $\langle x^2(\tau)\rangle$ approximately follows a power-law dependence on τ, $\langle x^2(\tau)\rangle \sim \tau^{\alpha}$. For pure diffusion in a viscous medium, $\alpha=1$, while if $\alpha<1$, the motion of the tracer particles is subdiffusive and elastic effects are present. Our results show that even for the earliest time studied (for which $t_w=1800$ s) the motion of the tracer particles is subdiffusive, that is, the mean-squared displacement increases more slowly than linearly with τ. As t_w increases, the material becomes more viscous and $\langle x^2\rangle$ decreases for a given lag time, but the slope α also decreases. For $t_w \gtrsim 4800$ s, $\langle x^2\rangle$ is small and almost independent of lag time, indicating that at this value of t_w and beyond, the tracer particles are almost immobile.

Figure 2 shows the effect of the aggregation time on $\langle x^2(\tau)\rangle$. The main plot in Fig. 2 shows $\langle x^2(\tau)\rangle$ plotted as a function of t_w for a few values of τ. Initially, $\langle x^2(\tau)\rangle$ decreases rapidly with t_w, but beyond a certain aggregation

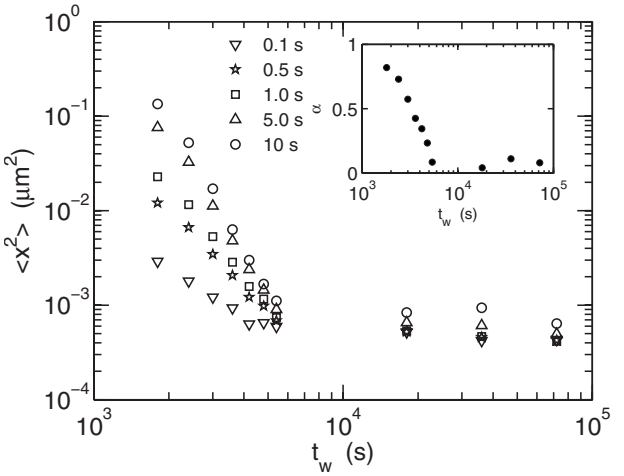

FIG. 2. The mean-squared displacement at selected lag times indicated by the different symbols as a function of t_w. The inset shows the dependence of the diffusive exponent α on the aggregation time.

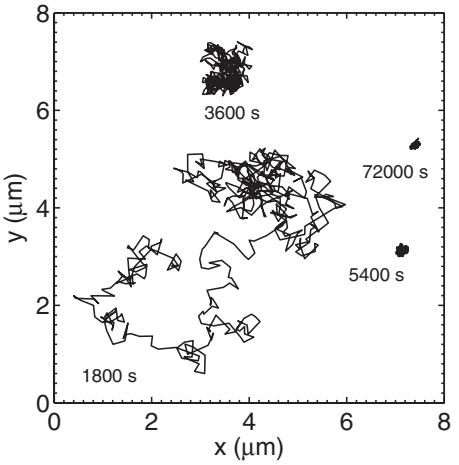

FIG. 3. Examples of tracer particle trajectories in Laponite for $t_w=1800$, 3600, 5400, and 72 000 s. The duration of the trajectories is 50 s.

time $t_w^{\star}$, which is again approximately 5000 s, the mean-squared displacement no longer changes with time. The rate of decrease of $\langle x^2(\tau)\rangle$ with time is higher at higher lag times, but the value of $t_w^{\star}$ is independent of τ within our measurement uncertainties. The inset to Fig. 2 shows the diffusive exponent α as a function of t_w. As noted above, α decreases steadily with t_w up to the same time $t_w^{\star}$, beyond which it becomes constant and close to zero.

Some sample trajectories of tracer particles at different stages of the aging process are shown in Fig. 3. In all cases the duration of the trajectories is 50 s. As t_w increases, the trajectories become more compact and localized as the particles become less mobile. At early stages ($t_w=1800$ s), the particles move almost freely, although the trajectory for this value of t_w shown in Fig. 3 spends a lot of time in one particular region before wandering elsewhere. This indicates that even at this time the motion is not completely random and is consistent with the subdiffusive behavior of $\langle x^2(\tau)\rangle$ seen in Fig. 1. At $t_w=3600$ s the motion of the tracer particle has become restricted to a particular region of the fluid about 1 μm across, of the same order as the particle size. For aggregation times greater than $t_w^{\star}$ ($t_w=5400$ and 72 000 s are shown in Fig. 3), the trajectories are very compact; the particles are effectively trapped and do not move significantly from their mean positions.

Figure 4 shows the distribution $P(\Delta x)$ of particle displacements $\Delta x=x(t+\tau)-x(t)$ at a lag time of $\tau=0.5$ s for $t_w=1800$ s [Fig. 4(a)] and $t_w=5400$ s [Fig. 4(b)]. For pure diffusion in a homogeneous material, the probability distribution of Δx would be a Gaussian. On the other hand, in a spatially heterogeneous medium, different particles will sample different regions of the fluid which have different local properties and the distribution will deviate from a Gaussian. Figure 4(a) shows that at early times the distribution is fairly well-described by a Gaussian, although there are slight but systematic deviations from the best-fit Gaussian at large Δx. At long times, as in Fig. 4(b), the deviations from a Gaussian distribution are much more pronounced, showing that the suspension is significantly heterogeneous on the scale probed by the tracer particles.

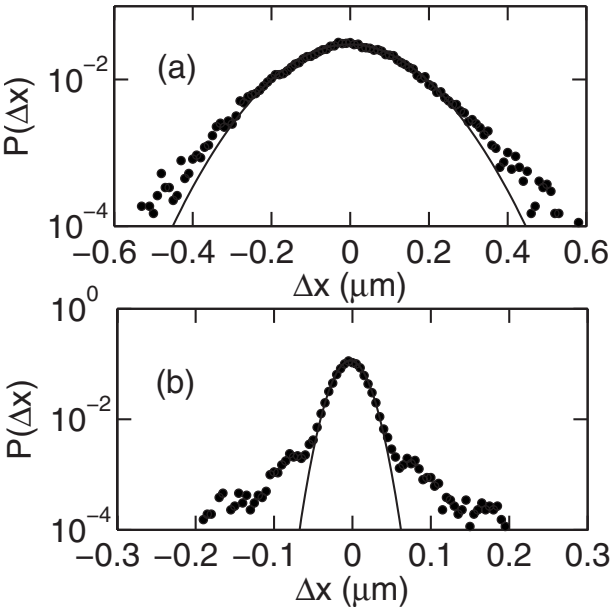

FIG. 4. The probability distribution of the distances moved by the tracer particles in a lag time of 0.5 s. The curves are Gaussian distributions fitted to the data. (a) $t_w=1800$ s and (b) $t_w=5400$ s.

The deviations from Gaussian behavior can be quantified using a non-Gaussian parameter N, defined in terms of the ratio of the fourth moment of $P(\Delta x)$ to the second moment [55]:

$$N = \frac{\langle \Delta x^4 \rangle}{3\langle \Delta x^2 \rangle^2} - 1. \tag{5}$$

$N=0$ for a homogeneous medium in which $P(\Delta x)$ is Gaussian, but is nonzero when the distribution deviates from Gaussian. The variation of N with t_w shown in Fig. 5 illustrates how the degree of heterogeneity of the sample changes with time. N initially increases sharply with t_w, but seems to approach a plateau value beyond $t_w^\star$. Within the experimental scatter, N is independent of lag time.

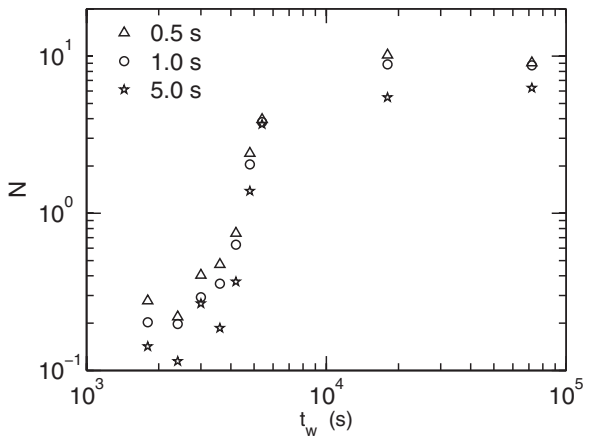

FIG. 5. The non-Gaussian parameter N plotted against the time since preparation of the Laponite sample. The different symbols represent different lag times.

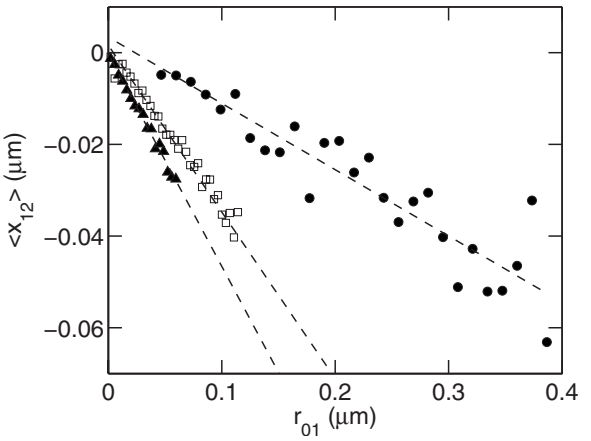

FIG. 6. The degree of correlation between successive particle displacements for a lag time of 0.5 s. t_w is 1800 s (closed circles), 3600 s (open squares), and 72 000 s (closed triangles). The dashed lines are fits of the data to a straight line, $\langle x_{12} \rangle = -br_{01}$. The slope of the fits gives the parameter b, which is a measure of the ability of the material to restrict the motion of the tracer particles.

To study the effect of the fluid structure on the motion of the spheres, we consider correlations between two successive displacements of equal lag time. Let $\vec{r}_{01}$ and $\vec{r}_{12}$ be the two-dimensional displacements of the particles in the plane of focus between times t_0 and $t_1=t_0+\tau$ and between t_1 and $t_2=t_1+\tau$, respectively, for some fixed lag time τ. If the motion of the particles is random, the direction of $\vec{r}_{12}$ will be uncorrelated with that of $\vec{r}_{01}$. On the other hand, if the particles are confined by the fluid's microstructure, then for sufficiently long lag times, successive displacements of a given particle will be negatively correlated—a particle which moves in a certain direction in one step has an increased probability of rebounding in the opposite direction on the next [46,47,56,57].

Figure 6 shows $\langle x_{12} \rangle$ plotted as a function of r_{01} for $\tau=0.5$ s and $t_w=1800$, 3600, and 72 000 s. Here $\langle x_{12} \rangle$ is the mean value of the projection of $\vec{r}_{12}$ in the direction of $\vec{r}_{01}$. In all cases, the data fall on a straight line with a negative slope. Deviations from linear behavior at a particular distance would indicate a characteristic size of the regions in which the particles are confined; the absence of any such deviations in Fig. 6 indicates the absence of any characteristic length scale in the microstructure over the range of distances probed by our experiments. The magnitude of the slope b is related to the ability of the fluid's microstructure to restrict the motion of the tracer particles, and so is a measure of the microscopic strength of the material. In Fig. 7, we show the dependence of b on $\langle x^2 \rangle^{1/2}$, the root-mean-squared displacement of the particles, for a number of different values of t_w. For samples with $t<t_w^\star$, b increases approximately linearly with $\langle x^2 \rangle^{1/2}$, that is, the further the spheres move, the more they are restrained by the structure in the fluid. Beyond the gel transition, however, the plot of b vs $\langle x^2 \rangle^{1/2}$ is essentially vertical: the particle is completely confined spatially by what looks like a square well potential due to the gel microstructure. The dependence of b on the aggregation time is shown for several different lag times in the inset to Fig. 7. We observe a steady increase of b with t_w up to the same critical

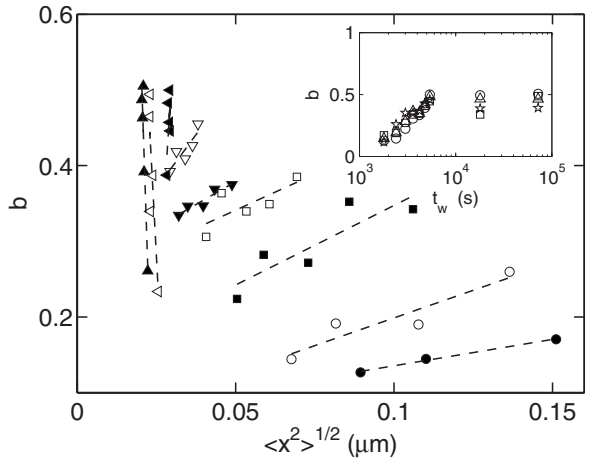

FIG. 7. A plot of the gel strength b of the Laponite suspension against the root-mean-squared displacement. The symbols correspond to different values of t_w as in Fig. 1. t_w increases from the lower right to the upper left of the graph. The dashed lines are linear fits to the data. The inset shows the gel strength as a function of t_w for lag times of 0.3 s (circles), 0.5 s (triangles), 1 s (squares), and 2 s (stars).

time $t_w^\star$, beyond which b becomes approximately constant. This behavior is independent of τ.

Figure 8 shows the micron-scale frequency-dependent viscous and elastic moduli of the fluid at four different values of t_w, calculated from the mean-squared displacement as outlined in Sect. II B above. For the youngest sample [t_w =1800 s, Fig. 8(a)], $G_m'' > G_m'$, and the material's behavior is predominantly viscous. At t_w=3600 s [Fig. 8(b)] G_m'' and G_m' are almost equal over the accessible range of frequencies and both show a power-law dependence on ω. For later times, as shown in Figs. 8(c) and 8(d), $G_m'' < G_m'$ and the material behavior is dominated by elasticity.

The bulk elastic modulus G_b' is plotted as a function of the strain amplitude γ in Fig. 9. In all cases, G_b' assumes a plateau value at low strain, corresponding to the linear viscoelastic regime. As γ is increased, however, G_b' starts to decease rapidly at a strain amplitude of approximately 0.15. We define the yield strain γ_y as that at which G_b' decreases to 80% of its initial plateau value, and calculate the yield stress σ_y as $\sigma_y = G_b'(\gamma_y)\gamma_y$. Our definition of γ_y is arbitrary but provides us with an internally consistent method of determining the yield stress for our samples. The inset of Fig. 10 shows γ_y as a function of t_w, and the apparent yield stress is plotted as a function of aggregation time in the main panel of Fig. 10. As expected, the yield stress of the suspension increases as time passes.

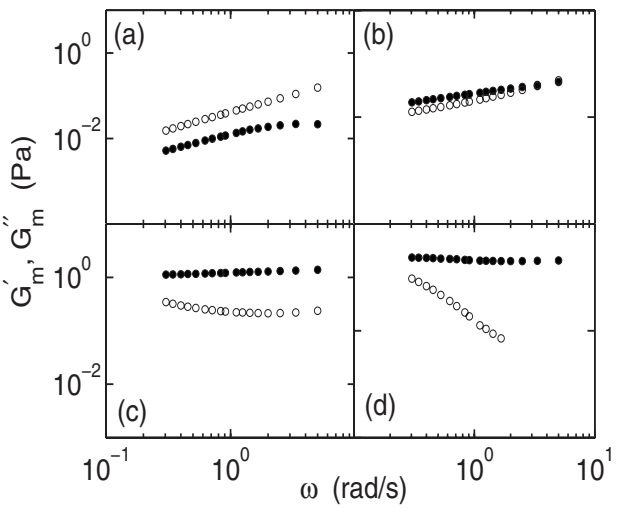

FIG. 8. The microscopic viscous (open circles) and elastic (closed circles) moduli calculated from $\langle x^2 \rangle$ using Eqs. (3) and (4), plotted as a function of frequency. The aggregation time is (a) 1800 s, (b) 3600 s, (c) 5400 s, and (d) 72 000 s.

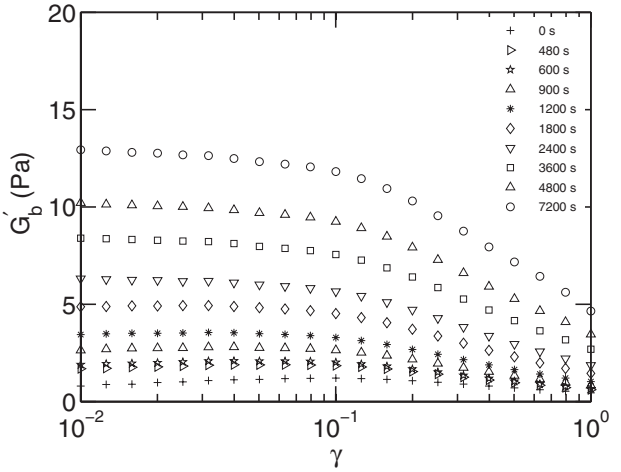

FIG. 9. The bulk elastic modulus G_b' of our Laponite suspension measured using oscillatory shear, plotted as a function of the strain amplitude. The symbols represent different values of t_w as indicated in the legend.

The bulk and micron-scale viscous and elastic moduli are compared in Fig. 11, where we plot G_b' and G_b''—determined from small amplitude oscillatory shear measurements with the rheometer—along with G_m' and G_m'', which are determined from analysis of the mean-squared displacement of the tracer particles. In both cases, the frequency is 1 rad/s.

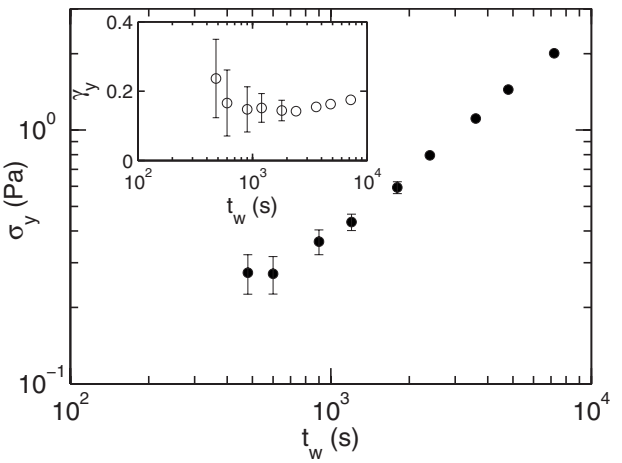

FIG. 10. The evolution of the apparent yield stress of the Laponite suspension with t_w. The yield stresses were calculated from the data in Fig. 9, as discussed in the text. The inset shows the yield strain γ_y.

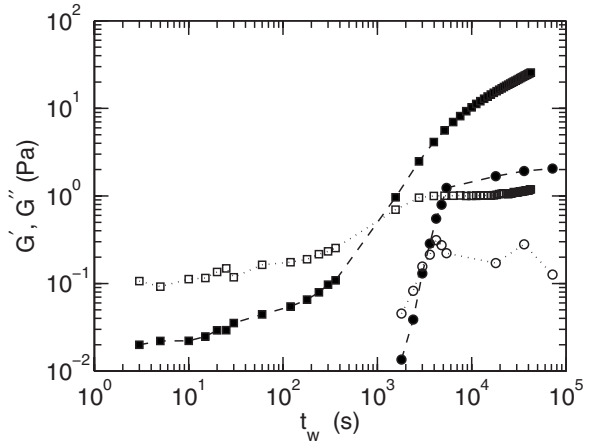

FIG. 11. A comparison of the bulk and microscopic viscoelastic moduli as a function of t_w. The squares are the bulk values G_b' and G_b'' measured with the rheometer using a strain amplitude of 0.05. Open symbols are G'' and solid symbols are G'. The circles are the microscopic moduli G_m' and G_m'' calculated from the particle-tracking data. The frequency for both sets of data is 1 rad/s.

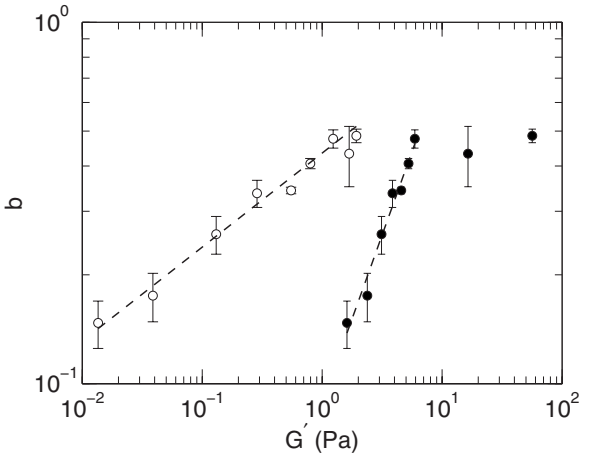

FIG. 12. The relationship between b, which is a measure of the gel strength on the micron scale, and the bulk (closed symbols) and microscopic (open symbols) elastic moduli. The data for b were averaged over results for three lag times, τ=0.3, 0.5, and 1.0 s, and the error bars indicate the standard deviations. The dashed lines are power-law fits to the data discussed in the text.

On both the microscopic and the bulk scales, the Laponite suspension is primarily viscous for low aggregation times. Both moduli increase as t_w increases, and there is a crossover time t_g at which the two moduli are equal; we identify this time with the gel point. On the bulk scale, the gel time $t_{g,b}$ is approximately 1000 s. The elastic modulus continues to increase steadily beyond the crossover, while the viscous modulus increases until $t_w \approx 3000$ s, then remains approximately constant. The gel point determined from the microscopic data is later—$t_{g,m}$ is about 3500 s. The microscopic elastic modulus increases fairly rapidly (roughly as t_w^4) until $t_w \approx 5000$ s (consistent with the value of $t_w^\star$ determined above), beyond which the rate of increase becomes much slower, while the viscous modulus remains constant within the experimental scatter for $t_w \gtrsim t_{g,m}$. Both of the macroscopic moduli are more than an order of magnitude larger than the corresponding effective micron-scale moduli.

In Fig. 12 we plot the microscopic gel strength b, determined from the correlation analysis described above, against both the bulk and the micron-scale elastic moduli. Since the measurements of $G_b'(t_w)$ were not necessarily made at the same values of the aggregation time as the particle-tracking measurements, the data for $G_b'(t_w)$ were fitted to a smooth curve and interpolated to obtain the modulus at the required values of t_w. On the bulk scale, the elastic modulus increases monotonically with t_w, as shown in Fig. 11. In contrast, b increases with t_w up to $t_w^\star$, beyond which it becomes constant, as shown in Fig. 7. This change in behavior of the gel strength shows up clearly at high t_w when b is plotted against G_b'. Below $t_w^\star$, we find $b \propto G_b'^{0.93 \pm 0.04}$, consistent with a linear relationship. The micron-scale elastic modulus G_m' also initially increases with aggregation time, but, like the gel strength b, becomes approximately constant at $t_w^\star$. Since both quantities plateau at the same aggregation time, this transition is not reflected in the plot of b against G_m' in Fig. 12, and the relationship between them is well-described by a power law with an exponent of 0.26 ± 0.04.

IV. DISCUSSION

Gelation occurs via a percolation transition at which the suspended colloidal particles aggregate to form a macroscopic cluster which spans the sample volume. The viscoelastic response of the sol state is dominated by viscosity, while the gel state is primarily elastic and exhibits a bulk yield stress. At the gel point, G' and G'' are equal and show a power-law dependence on frequency, the viscosity $\eta = G''/\omega$ diverges at ω=0, while the zero-frequency elastic modulus is zero [15,16]. Our measurements of the bulk viscoelastic moduli G_b' and G_b'' shown in Fig. 11 are consistent with this behavior and with previous studies on Laponite [24,29,41,51] and other materials. For small t_w the viscous modulus dominates. Both elastic and viscous moduli increase with t_w, with the elastic modulus increasing more rapidly as the gel point is approached. At $t_w = t_{g,b} \approx 1000$ s, the two moduli become equal, and we identify this aggregation time with the bulk gel point. Around the same time, we observe the development of a measurable bulk yield stress. Beyond the bulk gel point, the suspension is primarily elastic on the bulk scale, but both moduli continue to increase with time, albeit more slowly.

Our measurements of the diffusion of the suspended tracer particles, which probe the viscoelastic properties of the suspension at length scales up to the size of the particle, show that a gel transition also occurs on the microscopic scale. In the fluid state the tracer particles undergo subdiffusive motion and the suspension is primarily viscous on the micron scale: the effective viscous modulus determined from the mean-squared displacement dominates over the elastic modulus. As the suspension approaches the gel point, we observe a steady evolution of the microstructure of the suspension in the sol state, with the microstructure restricting the tracers' motion more and more as the gel transition is approached. The diffusive exponent α which characterizes the particles' motion decreases, while the spatial inhomogeneity of the material increases.

Although the microscopic viscous and elastic moduli both increase with t_w, the rate of increase of G'_m is greater and the material becomes progressively more elastic. From Fig. 11, the micron-scale moduli become equal at $t_{g,m} \approx 3500$ s, significantly later than the bulk gel point. Figure 8(b) shows both micron-scale moduli at $t_w = 3600$ s, slightly beyond $t_{g,m}$. Figure 8 suggests that exactly at $t_{g,m}$, the two moduli will be equal and show a power-law dependence on ω, with an exponent of approximately 0.5, over a large range of frequencies. Assuming that this behavior persists down to zero frequency, our data indicate that at $t_{g,m}$ the micron-scale viscosity $\eta_m = G''_m/\omega$ will diverge as $\omega \to 0$, while at earlier times G''_m is roughly linear in ω and the viscosity is finite. Similarly at $t_{g,m}$ the zero frequency elastic modulus will be zero, while at higher t_w it is nonzero. This behavior is completely consistent with what is expected at a gel point, but on the microscopic scale.

Beyond the micron-scale gel point, at $t_w = t_w^\star \approx 5000$ s, the suspended tracer particles become immobile to within the precision of our measurements. This indicates that a yield stress develops on the microscopic scale as well. Between $t_{g,m}$ and $t_w^\star$, the value of G'_m continues to increase rapidly. Above $t_w^\star$, G' increases much more slowly. On the other hand the microscopic viscous modulus G'' appears to increase only slightly beyond $t_{g,m}$, but then becomes independent of aggregation time within our experimental precision.

These results suggest that the time scale of the gelation process is length-scale dependent. On the scale of a millimeter, corresponding to our bulk rheometric measurements, the gel point is at $t_{g,b}$. The viscoelastic moduli and the yield stress of the bulk material continue to evolve after that time, reflecting continued development of the microstructure on smaller length scales. At the length scale of order the size of our suspended particles, that is, the length scale probed by our particle-tracking measurements, the gel point is at the later time $t_{g,m}$. The micron-scale properties again continue to evolve beyond that time, indicating further changes to the microstructure on even smaller scales. The time $t_w^\star$, beyond which our particle-tracking measurements show no further changes in material properties, may thus represent the gel time on an even smaller scale corresponding to the minimum measurable displacement of the tracers. Based on the smallest values of $\langle x^2(\tau) \rangle$ plotted in Fig. 1, this minimum displacement is approximately 0.02 μm, slightly smaller than the diameter of the Laponite disks. We plot the gel time as a function of length scale in Fig. 13. Given the crudeness of both the time and length scale estimates, the good agreement with the power-law fit shown in the figure is fortuitous, but the increase in gel time with decreasing length scale is nonetheless evident.

The bulk gel point is associated with the formation of a percolation aggregate that spans the sample. Prior to the gel transition, the suspension consists of many clay aggregates with a distribution of sizes within a fluid consisting of water and individual clay particles. Aggregates large compared to the size of the tracers restrict their motion, resulting in subdiffusive behavior and a nonzero elastic modulus, while aggregates much smaller than the particles contribute to the viscosity of the background fluid experienced by the particles. As the bulk gel point is approached, smaller aggregates link together, the motion of the tracer particles becomes more restricted, and both the elastic and viscous moduli increase. At the gel point, a large fractal percolation cluster forms and the material becomes predominantly elastic and develops a yield stress on the bulk scale. On the small scale, however, the suspension still contains many regions that remain in the fluid state locally; since the percolation cluster is a fractal, these fluid regions will have a wide distribution of sizes and no characteristic length scale. The suspended particles will continue to undergo restricted diffusion in these fluid regions despite the fact that the material is macroscopically a gel. As time passes, the aggregates continue to grow and the sol regions diminish in size, as reflected in the continued evolution of the bulk viscous and elastic moduli. Eventually fluid regions roughly the size of the suspended tracer particles will become spanned by gel aggregates which connect to the main percolation cluster, and at that time the motion of the tracer particles will reflect a gel transition on that length scale. Ultimately, the entire material becomes a solid and the particles become completely immobilized. The bulk-scale moduli increase more gradually than do the microscopic moduli. This may reflect the gradual build up of the macroscopic percolation cluster due to aggregation at all length scales, leading to a gradual strengthening of the bulk network. In contrast, the rapid increase of the micron-scale moduli indicates that gelation on the micron scale—which does not involve length scales larger than those probed by our tracer particles—occurs more abruptly.

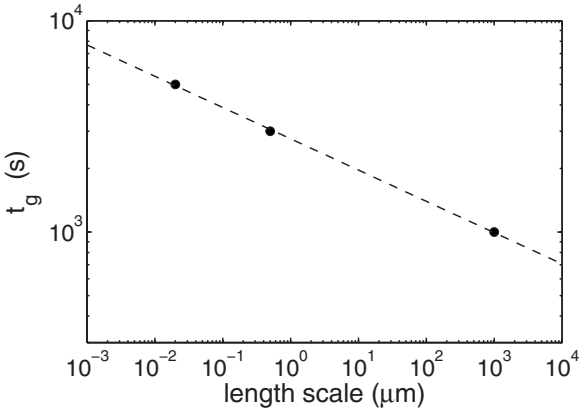

FIG. 13. The gel time t_g plotted against the length scale of the measurement. The dashed line is a power-law fit to the data which gives an exponent of -0.15 ± 0.05.

It is difficult *a priori* to distinguish between gel and glass phases in soft materials, and Laponite is known to exhibit both [7,8]. We identify the state we study as a gel for several reasons. Our particle-tracking data indicate that the state is inhomogeneous on the micron scale, as expected for a gel formed by an aggregation process. In contrast, the glass state is expected to be locally homogeneous [8,12,25]. We work at a relatively high ion concentration, at which the particle interactions will consist of a screened long-range electrostatic repulsion plus a short-range van der Waals attraction. In this regime, both experiments and simulations point to gelation by an aggregation process that leads to the formation of a

percolation cluster [12]. Our data suggest in two ways that the gel structure on the micron scale is fractal, as predicted by the percolation model. First, the power-law scaling of the moduli near the microscopic gel point is consistent with a fractal microstructure. Second, the absence of any deviations from linear behavior of the correlation data presented in Fig. 6 indicates that there is no characteristic length scale over the range of distances probed in our experiments.

Recently, Matsunaga and Shibayama studied the gelation of gelatin solutions as a function of temperature using both conventional rheometry and dynamic light scattering [19]. They found that the gel transition occurred at the same temperature on the length scale probed by their light scattering experiments as on the bulk scale (although small-angle neutron scattering experiments did not show a gel transition at the same temperature) [19]. This is not inconsistent with the results of the present paper: in the gelatin system, the temperature sets the strength of the interparticle interactions, and for a given interaction strength the entire material will eventually gel. What our results suggest is simply that the gelation does not occur on all length scales simultaneously. It would be interesting to study the kinetics of gelation in the gelatin system to confirm the generality of the present results.

A connection between the microscopic and bulk measurements is provided by the linear relationship between the gel strength b, a microscopic quantity, and the bulk elastic modulus G_b' shown in Fig. 12. At a given aggregation time, however, both the macroscopic viscous and elastic moduli are much larger than the corresponding microscopic moduli. Similar results have been obtained with Carbopol gels [46,47] and Gellan gum [49], although microrheological measurements have been shown to agree with bulk rheometry for poly(ethylene oxide) [3,58,59], a suspension of hard-sphere silica particles in ethylene glycol [3]; an oil-in-water emulsion [3,60], and crosslinked poly(acrylamide) [61]. Although it has been suggested that the observed differences may be due to chemical interactions between the probe particles and the material under study [49,62,63], we believe that, at least in the present case, they indicate a real difference between the rheological properties on the scale probed by the tracer particles and the bulk properties. The fact that we find the gel time to be quite different on the two scales supports this interpretation—this difference cannot be removed by simply scaling $\langle x^2(\tau)\rangle$, for example. In fact, when the size of the probe particles is similar to the length scale of the material's microstructure, the particles are only able to sample the local viscoelastic properties of the material rather than the mean, bulk properties, and thus it is not surprising that differences are observed.

V. CONCLUSION

We have studied the gelation of a colloidal suspension of Laponite clay particles using particle-tracking measurements and conventional shear rheometry. We have measured the evolution of the mechanical properties and the microscopic structure of the suspension as it gels. Our micron-scale measurements probe the local viscoelastic properties of the material rather than its bulk properties, and we observe that the viscoelastic moduli measured on the micron scale are substantially lower than the corresponding bulk-scale moduli. We observe a gel transition, defined by the time at which the viscous and elastic moduli become equal, on both the bulk and microscopic scales. Our results indicate that the transition is length-scale dependent: gelation occurs later on smaller length scales.

ACKNOWLEDGMENTS

The research was funded by NSERC of Canada. We are grateful to Dr. Stephen Sims for the use of his fluorescence microscope for the particle-tracking experiments.

[1] R. Larson, *The Structure and Rheology of Complex Fluids* (Oxford University Press, New York, 1999).
[2] P. Sollich, F. Lequeux, P. Hebraud, and M. E. Cates, Phys. Rev. Lett. **78**, 2020 (1997).
[3] T. G. Mason and D. A. Weitz, Phys. Rev. Lett. **74**, 1250 (1995).
[4] T. G. Mason, Rheol. Acta **39**, 371 (2000).
[5] I. Y. Wong, M. L. Gardel, D. R. Reichman, E. R. Weeks, M. T. Valentine, A. R. Bausch, and D. A. Weitz, Phys. Rev. Lett. **92**, 178101 (2004).
[6] T. A. Waigh, Rep. Prog. Phys. **68**, 685 (2005).
[7] H. Tanaka, J. Meunier, and D. Bonn, Phys. Rev. E **69**, 031404 (2004).
[8] B. Ruzicka, L. Zulian, R. Angelini, M. Sztucki, A. Moussaïd, and G. Ruocco, Phys. Rev. E **77**, 020402(R) (2008).
[9] D. Stauffer, A. Coniglio, and M. M. Adam, Adv. Polym. Sci. **44**, 103 (1982).
[10] D. Stauffer and A. Aharony, *Introduction to Percolation Theory* (Taylor and Francis, London, 1992).
[11] M. Djabourov, Polym. Int. **25**, 135 (1991).
[12] E. Zaccarelli, J. Phys.: Condens. Matter **19**, 323101 (2007).
[13] V. Prasad, V. Trappe, A. D. Dinsmore, P. N. Segre, L. Cipelletti, and D. A. Weitz, Faraday Discuss. **123**, 1 (2003).
[14] F. Chambon and H. H. Winter, Polym. Bull. (Berlin) **13**, 499 (1985).
[15] H. H. Winter and M. Mours, Adv. Polym. Sci. **134**, 166 (1997).
[16] H. H. Winter and F. Chambon, J. Rheol. **30**, 367 (1986).
[17] C. Schwittay, M. Mours, and H. Winter, Faraday Discuss. **101**, 93 (1995).
[18] E. R. Payro and J. L. Llacuna, J. Non-Cryst. Solids **352**, 2220 (2006).
[19] T. Matsunaga and M. Shibayama, Phys. Rev. E **76**, 030401(R) (2007).
[20] S. Richter, Macromol. Chem. Phys. **208**, 1495 (2007).
[21] J. E. Martin and J. P. Wilcoxon, Phys. Rev. Lett. **61**, 373

(1988).
[22] F. Pignon, J. Piau, and A. Magnin, Phys. Rev. Lett. **76**, 4857 (1996).
[23] M. Kroon, G. H. Wegdam, and R. Sprik, Phys. Rev. E **54**, 6541 (1996).
[24] M. Kroon, W. L. Vos, and G. H. Wegdam, Phys. Rev. E **57**, 1962 (1998).
[25] B. Ruzicka, L. Zulian, and G. Ruocco, Phys. Rev. Lett. **93**, 258301 (2004).
[26] H. Z. Cummins, J. Non-Cryst. Solids **353**, 3891 (2007).
[27] R. G. Avery and J. D. F. Ramsay, J. Colloid Interface Sci. **109**, 448 (1986).
[28] D. W. Thomson and J. T. Butterworth, J. Colloid Interface Sci. **151**, 236 (1992).
[29] A. Mourchid, A. Delville, and P. Levitz, Faraday Discuss. **101**, 275 (1995).
[30] A. Mourchid, A. Delville, J. Lambard, E. Lecolier, and P. Levitz, Langmuir **11**, 1942 (1995).
[31] F. Pignon, A. Magnin, J.-M. Piau, B. Cabane, P. Lindner, and O. Diat, Phys. Rev. E **56**, 3281 (1997).
[32] D. Bonn, H. Tanaka, G. Wegdam, H. Kellay, and J. J. Meunier, Europhys. Lett. **45**, 52 (1998).
[33] D. Bonn, H. Kellay, H. Tanaka, G. Wegdam, and J. Meunier, Langmuir **15**, 7534 (1999).
[34] A. Knaebel, M. Bellour, J. P. Munch, and V. Viasnoff, Europhys. Lett. **52**, 73 (2000).
[35] P. Levitz, E. Lecolier, A. Mourchid, A. Delville, and S. Lyonnard, Europhys. Lett. **49**, 672 (2000).
[36] B. Abou, D. Bonn, and J. Meunier, Phys. Rev. E **64**, 021510 (2001).
[37] M. Bellour, A. Knaebel, J. L. Harden, F. Lequeux, and J.-P. Munch, Phys. Rev. E **67**, 031405 (2003).
[38] S. Kaloun, R. Skouri, M. Skouri, J. P. Munch, and F. Schosseler, Phys. Rev. E **72**, 011403 (2005).
[39] D. R. Strachan, G. C. Kalur, and S. R. Raghavan, Phys. Rev. E **73**, 041509 (2006).
[40] J. Ramsay, J. Colloid Interface Sci. **109**, 441 (1985).
[41] S. Cocard, J. F. Tassin, and T. Nicolai, J. Rheol. **44**, 585 (2000).
[42] B. Abou, D. Bonn, and J. Meunier, J. Rheol. **47**, 979 (2003).
[43] C. Wilhelm, F. Elias, J. Browaeys, A. Ponton, and J.-C. Bacri, Phys. Rev. E **66**, 021502 (2002).
[44] S. Jabbari-Farouji, D. Mizuno, M. Atakhorrami, F. C. MacKintosh, C. F. Schmidt, E. Eiser, G. H. Wegdam, and D. Bonn, Phys. Rev. Lett. **98**, 108302 (2007).
[45] Y. Gao and M. L. Kilfoil, Phys. Rev. Lett. **99**, 078301 (2007).
[46] F. K. Oppong, L. Rubatat, B. J. Frisken, A. E. Bailey, and J. R. de Bruyn, Phys. Rev. E **73**, 041405 (2006).
[47] F. K. Oppong and J. R. de Bruyn, J. Non-Newtonian Fluid Mech. **142**, 104 (2007).
[48] H. A. Houghton, I. A. Hasnain, and A. M. Donald, Eur. Phys. J. E **25**, 119 (2008).
[49] M. Caggioni, P. T. Spicer, D. L. Blair, S. E. Lindberg, and D. A. Weitz, J. Rheol. **51**, 851 (2007).
[50] B. S. Neuman and K. G. Sansom, Isr. J. Chem. **8**, 315 (1970).
[51] A. Mourchid and P. Levitz, Phys. Rev. E **57**, R4887 (1998).
[52] J. Crocker and D. G. Grier, J. Colloid Interface Sci. **179**, 298 (1996).
[53] J. Crocker and E. Weeks, 1996, URL http://www.physics.emory.edu/~weeks/idl/.
[54] C. W. Macosko, *Rheology: Principles, Measurements and Applications* (Wiley, New York, 1994).
[55] W. K. Kegel and A. Blaaderen, Science **287**, 290 (2000).
[56] B. Doliwa and A. Heuer, Phys. Rev. Lett. **80**, 4915 (1998).
[57] E. R. Weeks and D. A. Weitz, Chem. Phys. **284**, 361 (2002).
[58] M. T. Valentine, P. D. Kaplan, D. Thota, J. C. Crocker, T. Gisler, R. K. Prud'homme, M. Beck, and D. A. Weitz, Phys. Rev. E **64**, 061506 (2001).
[59] B. R. Dasgupta, S. Y. Tee, J. C. Crocker, B. J. Frisken, and D. A. Weitz, Phys. Rev. E **65**, 051505 (2002).
[60] T. G. Mason, H. Gang, and D. A. Weitz, J. Mol. Struct. **383**, 81 (1996).
[61] B. R. Dasgupta and D. A. Weitz, Phys. Rev. E **71**, 021504 (2005).
[62] J. H. Shin, M. L. Gardel, L. Mahadevan, P. Matsudaira, and D. A. Weitz, Proc. Natl. Acad. Sci. U.S.A. **101**, 9636 (2004).
[63] J. Liu, M. L. Gardel, K. Kroy, E. Frey, B. D. Hoffman, J. C. Crocker, A. R. Bausch, and D. A. D. A. Weitz, Phys. Rev. Lett. **96**, 118104 (2006).